

Circuit design for multi-body interactions in superconducting quantum annealing system with applications to a scalable architecture

N. Chancellor^{†,1,*}, S. Zohren^{†,2} and P. A. Warburton^{1,3}

¹*London Centre for Nanotechnology 19 Gordon St, London, UK*

²*Department of Materials and Department of Engineering Science, University of Oxford, Parks Road, Oxford, UK*

³*Department of Electronic and Electrical Engineering, UCL, Torrington Place, London, UK*

** Current Affiliation: Department of Physics, Durham University, South Road, Durham, UK*

† Authors contributed equally.

(Dated: November 5, 2018)

PACS numbers:

Quantum annealing provides a way of solving optimization problems by encoding them as Ising spin models which are implemented using physical qubits. The solution of the optimisation problem then corresponds to the ground state of the system. Quantum tunnelling is harnessed to enable the system to move to the ground state in a potentially highly non-convex energy landscape. A major difficulty in encoding optimization problems in physical quantum annealing devices is the fact that many real world optimisation problems require interactions of higher connectivity as well as multi-body terms beyond the limitations of the physical hardware. In this work we address the question of how to implement multi-body interactions using hardware which natively only provides two-body interactions. The main result is an efficient circuit design of such multi-body terms using superconducting flux qubits. It is then shown how this circuit can be used as a unit cell of a scalable architecture by applying it to a recently proposed embedding technique for constructing an architecture of logical qubits with arbitrary connectivity using physical qubits which have nearest-neighbour four-body interactions.

Introduction – Solving machine learning and optimization problems by casting them as an Ising spin glass and then using a physical device to take advantage of quantum fluctuations has been a subject of much recent interest [1–9]. This interest is due in a large part to demonstration of the underlying principles of quantum annealing in condensed matter systems [10] and the more recent development of a programmable annealing device by D-Wave Systems Inc.[11, 12].

Mapping real world problems, or indeed even problems with a similar difficulty to interesting real world problems to a programmable annealer is a major practical challenge [13, 14]. It is known for example that even though finding the ground state of the native so-called Chimera graph of the D-Wave device is NP-hard, typical

randomly generated instances on this graph are actually easy to solve by simulated annealing type algorithms [15]. Because it is non-planar, minor embedding can be used to map a fully connected graph to the chimera, although at a significant overhead [16, 17].

The NP-completeness of finding the ground state of an arbitrary (2-body) Ising spin glass and therefore a chimera graph guarantees that any NP-complete problem can be mapped to finding the ground state of a Hamiltonian which is a subgraph of a chimera with polynomial overhead. For examples of how this can be done in practice, see [18, 19]. However, there is no indication that this approach is optimal. For problems which require higher order, (in the number of bits subject to a single clause) a mapping must be found from a Higher Order Binary Optimization (HOBO) to a Quadratic Unconstrained Binary Optimization problem (QUBO) [19].

In this letter, and a related work [20] we examine an alternative architecture, in which higher order problems can be express natively by coupling logical qubits to a group of ancilla. This letter will focus on native circuit implementations of this architecture, while [20] examines how the same principles can be applied within the Chimera architecture.

Implementing a single logical clause using the methods of [18, 19], would require the construction of a penalty function (up to an unimportant energy offset) on a set of logical qubits, where the penalty is 0 if the clause is satisfied and bigger or equal to a penalty weight g if the clause is violated. In the ideal case g should be infinite, but in practice its maximal value is limited by the hardware.

This function gives a generally different penalty to all “wrong” answers (i.e. the ones with the wrong parity), so the ground state of superpositions of more than one (i.e. a sum of multiple penalty functions on overlapping subsets of bits) of these penalty functions is meaningful if there exists a solution which violates 0 or only 1 of the clauses. In the 3-SAT example in [18], this kind of superposition is acceptable because the problem is cast as a decision problem of whether a state exists which

satisfies all of the penalties, however under a simple generalization of the problem to max-3-SAT, where we ask what is the choice which violates the least number of the constraints, this kind of superposition no longer yields a valid expression of the problem. In this case, like the parity check codes considered in [19], the only penalty based option is to express the entire optimization problem as one monolithic penalty, which can be computationally intensive.

Our proposal on the other hand is to construct a function which reproduces the spectrum of a high order penalty term, which is equal to 0 if the clause is satisfied and exactly equal to the penalty weight g if the clause is violated.

Because all states which violate the clause are penalized equally, the ground state of a superposition of an arbitrary number of such terms will in fact be the state which violates the smallest number of clauses, regardless of how many can be simultaneously satisfied. In general it may also be interesting to penalize different violations differently, but in a controlled way, our method also supports this.

As an example of how these techniques can be used, we explicitly show how to construct superconducting circuits which realize the architecture recently proposed in [21] as an alternative to the chimera graph with minor embedding. We discuss that this architecture allows us an additional freedom in choosing the annealing path which is not a feature in the current D-Wave device architecture. For simplicity, and because it is what is required for the architecture in [21], we will restrict ourselves to discussing how to reproduce the classical spectrum of multi-body operators of the form $\mathcal{H}_N = J_N \sigma_1^z \dots \sigma_N^z$. Such multi-body terms are important for many applications. For example, it is well-known that spin glasses undergo a transition in complexity when moving from 2-body couplings to multi-body terms of order 3 and higher [22–24]. In this transition the number of extrema of the energy landscape grows from a polynomial function in the number of spins to an exponential function in the number of spins, where at the same time a banded structure in energy appears for saddle points of various orders [23]. The latter has various implications for example for energy landscapes of deep neural networks which are related to spin glasses and where the order of the multi-body term of the spin glass is given by the depth of the network [25, 26].

Theoretical framework – As discussed above, in many foreseeable applications for adiabatic quantum computation, one needs implementations of interactions with multi-body term. Those interactions are of the type

$$\mathcal{H}_N = J_N \sigma_1^z \dots \sigma_N^z. \quad (1)$$

However, the architecture used in quantum annealing devices generally only allows for two-body interactions,

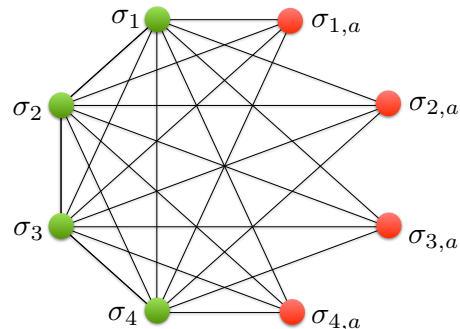


FIG. 1: Graph showing the connectivity of the Hamiltonian (3) for $N = 4$. The green vertices represent the logical qubits while the red vertices represent the ancillas. The logical qubits are fully connected amongst themselves with two-body couplings, represented as edges, of strength J . Each ancilla is connected to every logical qubit with two-body couplings of strength J^a .

Logical qubit states	Ancilla state	E
↑↑↑↑	↓↓↓↓	$+J_4$
↓↑↑↑, ↑↓↑↑, ↑↑↓↑, ↑↑↑↓	↑↓↓↓	$-J_4$
↓↓↑↑, ↓↓↑↓, ↓↑↑↓, ↑↓↑↑, ↑↓↑↓↑, ↑↑↓↓	↑↑↓↓	$+J_4$
↑↓↓↓, ↓↑↓↓, ↓↓↑↓, ↓↓↑↑	↑↑↑↓	$-J_4$
↓↓↓↓	↑↑↑↑	$+J_4$

TABLE I: Illustration of the various states of the 4-body term $\mathcal{H}_4 = J_4 \sigma_1^z \sigma_2^z \sigma_3^z \sigma_4^z$. Shown are the states of the logical qubits, the minimum energy states of the ancillas and the total energy.

leading to Hamiltonians of the form

$$\mathcal{H} = \sum_{i \sim j} J_{ij} \sigma_i^z \sigma_j^z + \sum_i h_i \sigma_i^z \quad (2)$$

where the first sum is taken over all adjacent qubits in the connectivity graph of the architecture.

We now describe a construction which reproduces the low-energy spectrum of (1) using a Hamiltonian with two-body interaction of the form of (2) including additional ancilla qubits. This is first done on a theoretical level and in the next section we present an efficient circuit design of this construction.

In particular, the Hamiltonian which reproduces the spectrum of the N -body term in (1) constitutes N logical qubits which are fully connected and an additional N ancilla qubits which are connected to all logical qubits but not amongst each other. This is illustrated in Figure 1 for the explicit case of a $N = 4$. The reason behind this construction will become apparent below. However, we can already deduce that if this construction was to reproduce the low energy spectrum of (1), then by symmetry the logical qubits must all have equal magnetic fields, h , as well as equal two-body couplings, J , amongst each

other. The same is true for the two-body couplings between the logical qubits and the ancillas, here denoted by J^a . This leads to the following Hamiltonian

$$\begin{aligned} \mathcal{H}_N^{(2)} = & J \sum_{i=1}^N \sum_{j=1}^{i-1} \sigma_i^z \sigma_j^z + h \sum_{i=1}^N \sigma_i^z + \\ & + J^a \sum_{i=1}^N \sum_{j=1}^N \sigma_i^z \sigma_{j,a}^z + \sum_{i=1}^N h_i^a \sigma_{i,a}^z. \end{aligned} \quad (3)$$

It is clear from (2) that the energy penalty of \mathcal{H}_N only depends on the number of up spins amongst σ_1^z to σ_N^z . Let us denote the number of up states by s . Then the energy is $+J_N$ if $N - s$ even and $-J_N$ if $N - s$ is odd. To reproduce this spectrum, we first choose the magnetic fields on the ancillas such that if there are s logical qubits in the up state there will be s ancillas in the down state. This can be achieved as follows: Consider $J^a > 0$, then since the effective mean magnetic field of the logical qubits on the ancillas is $J^a(2s - N)$, choosing $h_i^a = -J^a(2i - N) + q_i$ with $0 < q_i < J_a$ the ground state of the ancillas will have the first s ancillas in the down state and the remaining ones in the up state. For this work it is important that J^a is sufficiently large to enforce the condition that the ancillas are in their corresponding ground state. One can then fix the couplings in (3) to reproduce the spectrum of (1). In particular, the energy gap of a transition from s to $s + 1$ in (1) is $-2J_N$ if $N - s$ even and $+2J_N$ if $N - s$ is odd. Equating this with the same energy gap for (3), with $J^a \gg |J_N|$ sufficiently large to ensure that the ancillas are in their ground state, yields

$$\begin{aligned} J &= J^a, \quad h = -J^a + q_0 \\ q_i &= \begin{cases} +J_N + q_0 & N - i \text{ is odd,} \\ -J_N + q_0 & N - i \text{ is even,} \end{cases} \end{aligned} \quad (4)$$

with any q_0 which satisfies $|J_N| < q_0 \ll J^a$. The Hamiltonian (3) with coupling assignments (4), up to an overall constant energy offset, precisely reproduces the low energy spectrum of the Hamiltonian (1). This is assured for the part of the spectrum with $|\mathcal{H}_N| \ll J^a$. Once $|\mathcal{H}_N| \sim J^a$ the ancillas will no longer be in their corresponding ground state and the construction breaks down. Thus the range of the spectrum which can be reproduced using the above construction depends on the maximal coupling strength of the quantum annealing device in questions.

The above construction can be used for example to minor embed multi-body terms in already existing architectures such as the one produced by D-wave Systems Inc, as we show in a related work on message decoding problems on the D-wave device [20]. In this case the fully connected graph shown in Figure 1 must be obtained from a minor embedding [16] in the Chimera

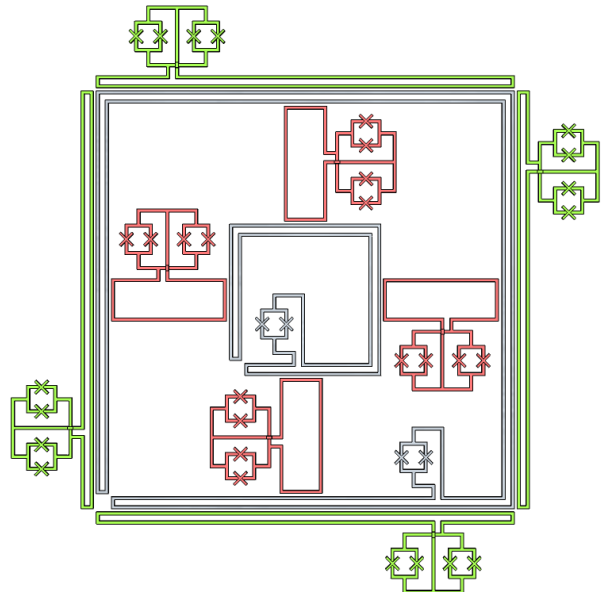


FIG. 2: Drawing of the circuit which implements the low energy spectrum of a 4-body coupler. The 4-logical qubits appear as the 4 (green) circuits on the perimeter, with a large loop (grey) coupling them together. Further in is a set of 4 ancilla qubits (red), which in turn themselves are coupled by an inner most loop (grey), which counteract the couplings induced from the outer loop. Note that the qubits are compound-compound Josephson junction circuits, while the couplers are simply compound.

graph. This is done using strong minor embedding couplings of strength J^m to “identify” qubits. This introduces a third energy scale into the problem and one must ensure that $|J_N| \ll J^a \ll J^m$.

Circuit implementing of multi-body interactions – In the previous section we presented an implementation which reproduces the low energy spectrum of multi-body terms using a system which only has two-body interactions. While it is possible to use minor embedding techniques to implement the above construction in already existing architectures such as D-wave, it can moreover be used to design a purpose build circuit for multi-body terms. As we will show below, the fact that both logical qubits as well as ancillas have all couplings of the same strength, permits a very efficient circuit implementation.

In particular, in this section we present a circuit implementation of a unit cell consisting of 4 logical qubits coupled through a 4-body interaction. In the following section we then show how to use the unit cell to build a scalable architecture.

To implement the fully connected graph between the logical qubits as well as the coupling between the logical qubits and the ancillas, we first inductively couple all of the qubits, both logical and ancilla, to a large loop. We demonstrate later that this arrangement produces the

desired graph up to the relevant order in perturbation theory. This loop is the outer loop in Figure 2. This coupler however also produces unwanted coupling terms between the ancillas, to cancel these off, we must add an additional loop, the inner loop in Figure 2, which can be biased with equal magnitude and opposite sign as the outer coupling loop to cancel the undesirable coupling between the ancillas.

The circuit design shown in Figure 2 requires that more than 2 qubits can be coupled using the same rf-SQUID couple design as presented in [27]. We demonstrate that to the same relevant order as used in the expansion in that paper, a group of qubits all inductively coupled to the same superconducting circuit realizes a fully connected 2-body graph of couplers between all of the qubits. Following [27], the energy for such a circuit with a coupler c and n qubits including Josephson and magnetic terms is

$$U = -E_c \cos \phi_c - \sum_{i=1}^n E_i \cos \phi_i + \frac{1}{8e^2} (\vec{\phi} - \vec{\phi}^x)^T \mathbb{L}^{-1} (\vec{\phi} - \vec{\phi}^x) \quad (5)$$

where $\vec{\phi}$ is a vector of the junction phases, $\vec{\phi}^x$ is the phase introduced by an external flux and the inductance matrix \mathbb{L} is given by,

$$\mathbb{L} = \begin{pmatrix} L_c & -M_{1c} & M_{2c} & \cdots \\ -M_{1c} & L_1 & 0 & \cdots \\ M_{2c} & 0 & L_2 & \ddots \\ \vdots & \vdots & \ddots & \ddots \end{pmatrix}. \quad (6)$$

This expression can easily be inverted to obtain the term \mathbb{L}^{-1} in the above expression up to $O(M^2)$. Following [27], we choose the bias fluxes such that,

$$\vec{\phi}^x = \begin{pmatrix} \phi_c^x \\ \pi + (M_{1c}/L_1)(\phi_c^{(0)} - \phi_c^x) \\ \pi + (M_{2c}/L_2)(\phi_c^{(0)} - \phi_c^x) \\ \vdots \end{pmatrix}. \quad (7)$$

It is now worth noting that if we choose any pair of qubits $i \neq j$ and separate out only terms in (5) which contain ϕ_i and/or ϕ_j , these equations will be identical to those found in [27]. These equations can therefore be solved independently in exactly the same way as that paper did resulting in,

$$U = const + \sum_{i=1}^{n-1} \sum_{j>1}^n \frac{M_{ic} M_{jc}}{4e^2 L_c L_i L_j} (\phi_i^{(0)} - \pi)(\phi_j^{(0)} - \pi), \quad (8)$$

which is exactly the formula of a set of couplings realizing a fully connected graph between all of the qubits. These

couplings are collectively tuneable with ϕ_c^x , but cannot be addressed individually. For our design we desire all $L_1 = L_2 = \dots = L$ and $M_{1c} = M_{2c} = \dots = M$, however as we will show, it is possible to tune for some types of slight imperfections in these values in for a real device.

Our realization of a multi-qubit fully connected effective 2-body graph is based on an experimentally proven design for a single coupler, for this reason many of the design problems have already been solved [27]. One issue which will effect our design differently is mismatches in the inducting couplings between the qubits and the loops. For a single coupler between two qubits it is not important for the mutual inductances to be matched, the coupling strength is simply proportional to a product of the mutual inductances between the two qubits and the coupler, regardless of whether or not they are equal. For our designs on the other hand, mismatches in the mutual inductances on the large loop will lead to different coupling strengths which can be viewed as effective spurious couplings between the logical bits and/or ancilla.

Let us first consider the effect of mismatches between the ancilla mutual inductances. The effect of these will be twofold, firstly, mismatched inductances will lead to imperfect cancelation of the couplings between the ancilla. If these spurious couplings are weak, they will not affect which ancilla are flipped, and just add a predictable (i.e. independent of which exact logical bits are up) energy penalty in exactly the same way as the ancilla fields which are used to enforce the effective couplers. Secondly, mismatches in these couplings will mean that the couplings between each ancilla and the logical qubits will be different (although identical for a given ancilla). Again, if the mismatches are small these can be corrected for with a slight modification to the ancilla fields.

We have shown above that small mismatches in the mutual inductances between the ancilla and the coupling loops are rather benign and can be easily corrected for. Unfortunately, mismatches in the inductances between the logical bits and the coupling loops are harder to correct for. Firstly, these will lead to effective couplings between logical bits and secondly to mismatches in the couplings between logical bits and ancilla. Neither of these can be tuned out by modifying the fields on the ancillas, so care must be taken to make sure that these inductances match to within experimental tolerances, possibly by placing additional compound Josephson junction loops near the interfaces between the logical qubits and the coupler loops to act as tuners by partially shielding or enhancing flux and thus tuning the mutual inductance.

The previous paragraph hints at an important aspect of this design, the requirements on the ancilla are much less strict than those on the logical qubits. In addition to not requiring precisely tuned mutual inductances, the ancilla need not be read out at the end of the annealing run. Furthermore, there is no reason to which the ancillas need to be run on the same annealing schedule

as the logical qubits. This presents a significant advantage, the annealing schedule in this architecture naturally breaks down into a path in a space defined by 2 parameters. Adjusting the annealing parameter, the ratio between the longitudinal and transverse fields, on the ancillas adjusts how strongly the multi-body constraints are enforced. The annealing parameter on the logical bits on the other hand acts analogously to the way it does in the standard 2-body transverse field Ising model.

This natural breakdown into two independent annealing parameters allows for several interesting possibilities. For one this provides a natural testbed for an optimizable annealing schedule. Secondly, by introducing a control element which acts non-deterministically, a device could be designed which anneals on a different schedule each run. If a pathological region (for example one with a very small gap) exists in the annealing trajectory space, such a protocol may be able to avoid this region during some of the runs, thereby increasing the robustness of the annealing algorithm.

Applications to construct a scalable architecture – We now show how our above circuit design can be used to construct a scaleable architecture using a recently proposed embedding techniques [21] which maps M logical qubits with full connectivity to $K = M(M-1)/2$ physical qubits which have 4-body nearest neighbour interactions (see Figure 3 (a)). More concretely, in [21] a model with 2-body interactions but arbitrary connectivity is considered

$$\mathcal{H} = \sum_{i=1}^M \sum_{j<i} J_{ij} \sigma_i^z \sigma_j^z, \quad (9)$$

where qubits are on a fully connected graph and we left out the magnetic fields for simplicity. We see that we have $M(M-1)/2$ degrees of freedom in the assignment of the couplings J_{ij} . In the embedding proposed in [21] the system is mapped to a system with $K = M(M-1)/2$ physical qubits $\tilde{\sigma}_i^z$ arranged in a pattern as shown in Figure 3 (a), where the K original couplings J_{ij} map on the K magnetic fields \tilde{b}_i of the physical qubits. The original qubits are associated with M four-body interactions, shown as plaquette in Figure 3 (a). The resulting Hamiltonian is

$$\mathcal{H} = \sum_{i=1}^K \tilde{b}_i \tilde{\sigma}_i^z - C \sum_{(i,j,k,l) \in \text{plaquettes}} \tilde{\sigma}_i^z \tilde{\sigma}_j^z \tilde{\sigma}_k^z \tilde{\sigma}_l^z \quad (10)$$

In Figure 3 (b) we illustrate how such an architecture can be physically implemented using our circuit design of a four-body term. The resulting architecture is scalable in the sense that adding a new logical qubit, simply amounts to adding a new row at the bottom. The final row is also used for readout of the values of the logical qubits as explained in [21].

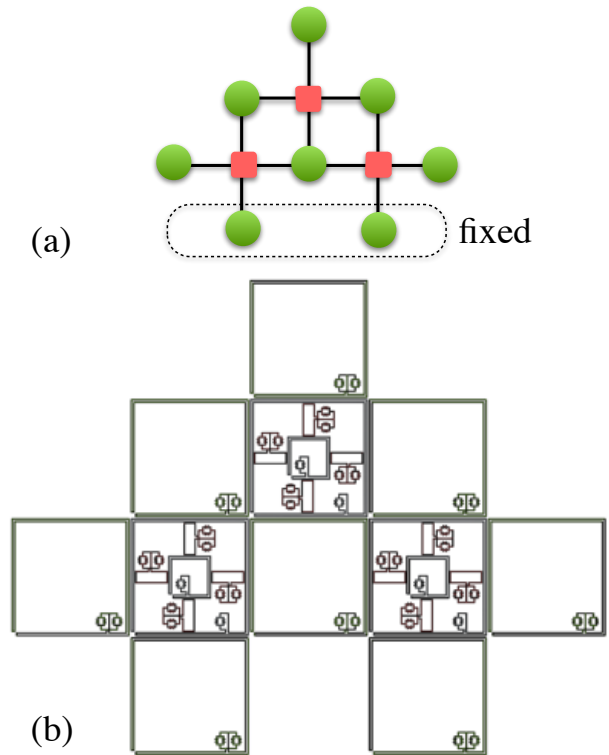


FIG. 3: (a) Schematically illustration of the embedding technique proposed in [21]. Shown is an embedding for $M = 3$ logical qubits whose interactions are mapped onto $K = 6$ physical qubits (green). Besides the 6 physical qubits encoding the interactions, there are an additional 2 physical qubits which enforce the boundary condition. The physical qubits are coupled using four-body interactions as illustrated by the plaquette (red). (b) A physical circuit implementation of the above embedding using our circuit design of a four-body term as presented in the previous section. The four qubits surrounding the four-body circuit are extended to couple to neighbouring four-body circuits. This presents a concrete circuit design for a scalable quantum annealing architecture using superconducting qubits.

Combining the embedding proposed in [21] with the circuit design for four-body interactions between rf-SQUIDS as described in the previous sections provides a concrete implementation for a scalable architecture allowing for two-body interactions of arbitrary connectivity. Interactions between rf-SQUIDS are mediated by the simple circuit design described above which involves at maximum couplings between 5 loops.

Discussion – Overcoming the physical limitations on connectivity and multi-body interactions of the underlying Ising spin system in hardware implementations of quantum annealing devices is a major challenge. In this work we present a method of effectively implementing Hamiltonians with multi-body terms by reproducing its low energy spectrum using Hamiltonians which only involve two-body interactions and a number of ancilla

qubits. While this construction can be used as a minor-embedding technique for existing quantum annealing architectures as we explore in a forthcoming work [20], the major result of this work is an efficient circuit design of the construction using superconducting flux qubits. Having the possibility of inductively coupling a number of qubits with all-to-all couplings of equal strength using a single coupling loop enables us to implement the multi-body terms using a very efficient circuit design. In the last section we show concretely how this circuit can be used as a unit cell for a scalable architecture using a recent embedding technique [21] which encodes logical qubits of arbitrary connectivity using physical qubits with nearest-neighbour four-body interactions.

As a final remark, let us mention that here we have focused on circuit based implementations of multi-body terms in the z -basis, i.e. $\sigma_1^z \dots \sigma_N^z$. This is natural, since the optimization problem is encoded in the z -basis. However, one can in principle also consider similar constructions in the basis of the transverse magnetic field, i.e. $\sigma_1^x \dots \sigma_N^x$, thereby enabling implementation of non-stoquastic Hamiltonians [28] involving multi-body terms. We leave such an analysis for future work.

The authors would like to thank Simon Benjamin and Stephen Roberts for discussions. NC and PW were supported by Lockheed Martin and by EPSRC (grant refs: EP/K004506/1 and EP/H005544/1). S.Z. acknowledges support by Nokia Technologies, Lockheed Martin and the University of Oxford through the Quantum Optimisation and Machine Learning (QuOpal) Project.

-
- [1] B. O’Gorman, et al., *Bayesian network structure learning using quantum annealing*, European Physical Journal-Special Topics 224 163 (2015).
- [2] H. Neven, et al. (2008). *Image recognition with an adiabatic quantum computer I. Mapping to quadratic unconstrained binary optimization*. arXiv:0804.4457 (2008).
- [3] S. Santra, et al., *Max 2-SAT with up to 108 qubits*, New Journal of Physics 16 045006 (2014).
- [4] I. Hen and A. P. Young *Solving the graph-isomorphism problem with a quantum annealer*, Phys. Rev. A 86 042310 (2012).
- [5] A. Perdomo-Ortiz, et al., *Finding low-energy conformations of lattice protein models by quantum annealing*, Scientific Reports 2 571 (2012).
- [6] S. Boixo, et al., *Evidence for quantum annealing with more than one hundred qubits*. Nature Physics, 10(3), 218-224 (2014).
- [7] D. Venturelli, et al., (2014). *Quantum optimization of fully-connected spin glasses*. arXiv:1406.7553.
- [8] E. Rieffel, et al., *A case study in programming a quantum annealer for hard operational planning problems*. Quantum Information Processing, 14(1), 1-36 (2015).
- [9] N. Chancellor, S. Szoke, W. Vinci, G. Aeppli and P. Warburton *Maximum-Entropy Inference with a Programmable Annealer*. arXiv:1506.08140 (2015).
- [10] J. Brooke, D. Bitko, T. F. Rosenbaum and G. Aeppli, *Quantum Annealing of a Disordered Magnet*, Science 284, p. 779-781 (1999)
- [11] W. M. Johnson, et al., *Quantum annealing with manufactured spins*, Nature 473 194 (2011).
- [12] R. Harris, et al., *Experimental investigation of an eight-qubit unit cell in a superconducting optimization processor*, Phys. Rev. B 82 024511 (2010).
- [13] I. Hen, et. al, *Probing for quantum speedup in spin glass problems with planted solutions*, arXiv:1502.01663 (2015).
- [14] H. G. Katzgraber, F. Hamze, Z. Zhu, A. J. Ochoa, and H. Munoz-Bauza *Seeking Quantum Speedup Through Spin Glasses: The Good, the Bad, and the Ugly* Phys. Rev. X 5, 031026 (2015).
- [15] H. G. Katzgraber, F. Hamze and R. S. Andrist, *Glassy Chimeras could be blind to quantum speedup: Designing better benchmarks for quantum annealing machines*, Phys. Rev. X 4, 021008 (2014).
- [16] V. Choi, *Minor-embedding in adiabatic quantum computation: II. Minor-universal graph design* Quantum Inf Process 10, 43353, (2011).
- [17] D. Venturelli, et al., *Quantum Optimization of Fully-Connected Spin Glasses* Phys. Rev. X 5, 031040 (2015).
- [18] V. Choi *Adiabatic Quantum Algorithms for the NP-Complete Maximum-Weight Independent Set, Exact Cover and 3SAT Problems* arXiv:1004.2226 (2004)
- [19] B. Zhengbing et. al. *Discrete optimization using Quantum Annealing on sparse Ising models* Frontiers in Physics 2 00056, (2014).
- [20] N. Chancellor, S. Zohren, P. Warburton, S. Benjamin, S. Roberts *A Direct Mapping of Max k-SAT and High Order Parity Checks to a Chimera Graph*, to appear (2016).
- [21] W. Lechner, P. Huke and P. Zoller, *A quantum annealing architecture with all-to-all connectivity from local interactions* (2015).
- [22] D. Sherrington, *Physics and Complexity: An Introduction*, in M. Delitala and G. Ajmone Marsan (eds.), *Managing Complexity, Reducing Perplexity*, Springer Proceedings in Mathematics and Statistics, 67, 119129 (2014).
- [23] A. Auffinger, G. Ben Arous and J. Cerny, *Random matrices and complexity of spin glasses*, arXiv:1003.1129 (2010).
- [24] C. K. Thomas and H. G. Katzgraber, *Optimizing glassy p-spin models*, Phys. Rev. E 83, 046709 (2011).
- [25] A. Choromanska, M. Henaff, M. Mathieu, G. Ben Arous and Y. LeCun, *The Loss Surfaces of Multilayer Networks*, arXiv:1412.0233 (2014).
- [26] L. Sagun, V. U. Guney, G. Ben Arous and Y. LeCun, *Explorations on high dimensional landscapes*, arXiv:1412.6615 (2014).
- [27] A. M. van den Brink, A. J. Berkley and M. Yalowsky *Mediated Tunable Coupling of Flux Qubits*, New Journal of Physics 7, 230 (2005)
- [28] S. Bravyi, et al., *The Complexity of Stoquastic Local Hamiltonian Problems*, Quant. Inf. Comp. 8, 0361 (2008)